Provided for non-commercial research and education use.
Not for reproduction, distribution or commercial use.

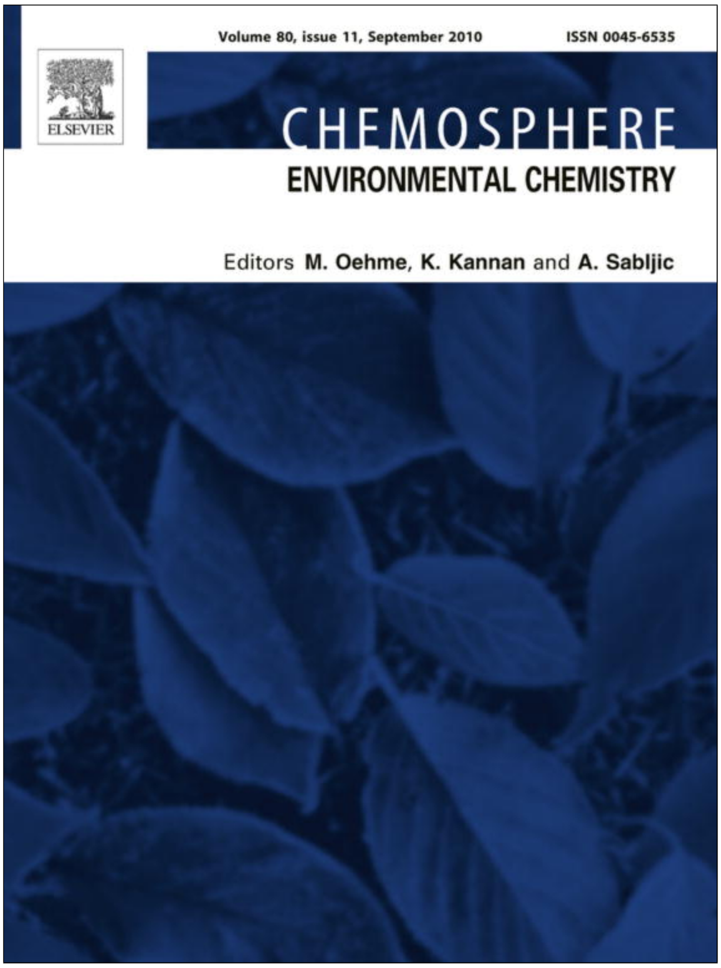
Volume 80, issue 11, September 2010
ISSN 0045-6535
ELSEVIER
CHEMOSPHERE
ENVIRONMENTAL CHEMISTRY
Editors M. Oehme, K. Kannan and A. Sabljic

This article appeared in a journal published by Elsevier. The attached copy is furnished to the author for internal non-commercial research and education use, including for instruction at the authors institution and sharing with colleagues.

Other uses, including reproduction and distribution, or selling or licensing copies, or posting to personal, institutional or third party websites are prohibited.

In most cases authors are permitted to post their version of the article (e.g. in Word or Tex form) to their personal website or institutional repository. Authors requiring further information regarding Elsevier's archiving and manuscript policies are encouraged to visit:

http://www.elsevier.com/copyright

Chemosphere 80 (2010) 1261–1267

Contents lists available at ScienceDirect

Chemosphere

journal homepage: www.elsevier.com/locate/chemosphere

Fluxes of PAHs from coal tar-impacted river sediment under variable seepage rates

Seunghun Hyun [a,]*, Hyun Park [b], Mi-Youn Ahn [c], Andrew R. Zimmerman [c], Chad T. Jafvert [d]

[a] *Division of Environmental Science and Ecological Engineering, Korea University, Seoul 136-713, Republic of Korea*
[b] *Korea Polar Research Institute, Incheon 406-840, Republic of Korea*
[c] *Department of Geological Sciences, University of Florida, Gainesville, FL 32611, USA*
[d] *School of Civil Engineering, Purdue University, West Lafayette, IN 47907, USA*

ARTICLE INFO

Article history:
Received 19 April 2010
Received in revised form 23 June 2010
Accepted 24 June 2010
Available online 16 July 2010

Keywords:
Coal tar
Sediment
Polycyclic aromatic hydrocarbons
Nonequilibrium
Seepage

ABSTRACT

The flux of several polycyclic aromatic hydrocarbons (PAHs) from coal tar-impacted river sediment was measured under various seepage rates in a laboratory scale. The batch PAH equilibrium data between aqueous phase (C_{eq}) and sediment phase was well-explained using a Raoult's law approach. In the flux measurement from column study, the steady-state PAH concentrations (C^{∞}) in the effluent solution were affected by a time-dependent nonequilibrium process; the seepage velocity was inversely proportional to the C^{∞} of PAH in the effluents. With a high seepage velocity of 4.06 cm d^{-1}, a large initial concentration was observed, possibly due to the greater disparity between C^{∞} and C_{eq}. This initial-flush export leveled off after a few pore volumes had been displaced. The chemical flux pattern of PAH was conceptually depicted by superimposing two analytical solutions, such as a slug lease followed by rate-limited solute lease. Under quiescent conditions, the sediment pore-water reached dissolution equilibrium with the solid phase. However, under dynamic groundwater seepage conditions, the seepage water flowing through sediment pores did not reach dissolution equilibrium, which was evidence of nonequilibrium dissolution. In conclusion, the mass flux of PAHs from coal tar-impacted sediment is determined by concurrent effect of the groundwater seepage rate and rate-limited PAH concentration in seepage water.

© 2010 Elsevier Ltd. All rights reserved.

1. Introduction

Coal tar, a non-aqueous phase liquid (NAPL), is composed of hundreds of aromatic organic compounds, including polycyclic aromatic hydrocarbons (PAHs), and a large number of other complex organic chemicals of undetermined identity (Luthy et al., 1994). Due to their carcinogenic and toxicological properties, PAHs are important coal tar-borne contaminants. During the last several decades, coal tar mixtures, a major byproduct when gas is produced from coal, have been accidentally spilled or improperly disposed of, thereby degrading the quality of nearby waters. Once coal tar reaches a water body, the light fractions form a pool on the top of the water table; whereas, the dense fractions migrate downward and form coal tar–sediment mixtures. Because several organic solutes can be released at various rates from the immobilized organic phase, coal tar-contaminated sediment can be a long-term source of groundwater and surface water contamination.

Dissolution is a primary mechanism controlling the flux of PAHs from coal tar-impacted sediment to the overlying water body. Because of this, many previous investigations have focused on the prediction of dissolution behavior of individual PAH compounds from the multi-component NAPL phase in various environmental settings. Parameters examined include the mole fraction of each compound (Heyse et al., 2002; Lee and Chrysikopoulos, 2006), residual NAPL saturation (Nambi and Powers, 2003), and porewater velocity (Seagren and Moore, 2003; Totsche et al., 2006). It has been shown that (1) the release of PAHs from the NAPL phase follows a dissolution process according to Raoult's law (Lee et al., 1992; Jafvert et al., 2006) and (2) dissolution may be rate-limited by intra-NAPL diffusion, rate-limited mass transfer, or slow release of PAHs from the immobile organic phase (Luthy et al., 1993). The non-homogenous distribution of PAHs in the NAPL phase has been frequently cited as an explanation for the observation of kinetic control on of aromatic hydrocarbon dissolution from petroleum-contaminated soils (Hunt et al., 1988a; Borden and Kao, 1992; Seagren and Moore, 2003; Totsche et al., 2006).

Dissolution experiments with single or multi-component NAPL ganglia have indicated that NAPL-aqueous phase equilibrium are rapidly achieved (Hunt et al., 1988b; Lee and Chrysikopoulos, 2006). However, for a field site with coal tar-contaminated river sediment or soil, such equilibrium conditions are rarely observed (Mahjoub et al., 2000; Heyse et al., 2002; Haritash and Kaushik,

---

* Corresponding author. Tel.: +82 2 3290 3068; fax: +82 2 953 0737.
E-mail address: soilhyun@korea.ac.kr (S. Hyun).

0045-6535/$ - see front matter © 2010 Elsevier Ltd. All rights reserved.
doi:10.1016/j.chemosphere.2010.06.064

2009). Thus, local equilibrium calculations clearly overestimate the effluent concentration, especially at higher seepage velocities.

In our previous studies, Hyun et al. (2006, 2007) investigated the behavior of equilibrium PAH dissolution and export flux due to upward groundwater seepage using coal tar-impacted river sediment collected from a former manufactured gas plant site. As a remediation strategy, the concept of a sand cap consisting of layers of permeable sand and gravel was proposed. However, it is unknown whether this type of cap will trap PAH contaminants or simply transfer them to the overlying water phase. In addition, the mass transfer potential of PAH from coal tar-impacted sediment will vary with spatiotemporal variations in groundwater efflux rates. This research was carried out in order to assess the impact of variation in the seepage rate on the release of PAH from coal tar sediment above which the sand cap was overlaid as a remediation technology. In order to evaluate the dissolving and/or exporting behavior of PAHs from coal tar-contaminated river sediment, laboratory columns packed with sediment with overlying sand at two different groundwater seepage velocities, and PAH in effluent was monitored over time. The concentration profile of PAHs in column effluent was interpreted using the concept of dissolution equilibrium and nonequilibrium between seepage water and coal tar-impacted sediment.

2. Materials and methods

2.1. Sediment and chemicals

A 122-cm core sample of coal tar-impacted river sediment was collected at a depth of 100 cm below the sediment surface from a river adjacent to a former manufactured gas plant site in Indiana, USA. Ottawa sand (20–30 mesh), used as a capping material, was purchased from Fluka. The particle density and bulk density of the sand were 2.65 g cm^{-3} and 1.88 g cm^{-3}, respectively and calculated effective porosity of 0.35. Standard PAH compounds of naphthalene, fluorene, phenanthrene, anthracene, fluoranthene and pyrene, all with >99% purity, were purchased from Sigma–Aldrich Chemical. The selected chemical and physical properties of the PAHs monitored in this study are listed in Table 1. Details of the sampling methods and sample characterization are reported elsewhere (Hyun et al., 2006).

2.2. Batch equilibrium partitioning

2.2.1. PAHs in sediment phase, C_{sed}

To determine the PAH concentrations in sediment, 10 g of wet sediment was extracted with 30 mL of a methanol and dichloromethane mixture (4:11, v/v) and placed on a rotary shaker at 50 rpm for 24 h. The sediment–solvent mixture was centrifuged at 3000 rpm for 20 min, and then the solutes in supernatant were extracted with hexane at the ratio of 10:1. A 1 mL aliquot was transferred to a glass amber vial for GC–FID analysis.

2.2.2. PAHs in aqueous phase, C_{eq}

To determine the PAH concentrations in aqueous solution equilibrated with the sediment, approximately 20 g of wet sediment was mixed with 200 mL of 5 mM $CaCl_2$ solution. Sediment-solution samples were briefly vortexed and then rotated end-over-end for 48 h. After settling for l h, the supernatants were transferred into 35 mL Teflon-capped centrifuge tubes. The tubes were centrifuged at 3000 rpm for 30 min and 2 mL aliquots of supernatant were transferred into glass amber vials. The PAHs, naphthalene, fluorene, phenanthrene, anthracene, fluoranthene and pyrene, were determined using HPLC–UV/FL analysis. Although over 40 PAH compounds were found in this sediment when extracts were concentrated and analyzed by GC–FID, only these specific compounds were monitored in the column experiments because the aqueous concentrations of these compounds in column effluent were sufficiently large that only small volume aliquots were required for analysis.

2.3. One-dimensional column displacement experiment

Column experiments were performed to assess the dissolution of PAHs from coal tar-contaminated sediment overlain by sand layers under saturated conditions as a function of advective water flux rates. A sketch of the soil column setup is given in Fig. 1. Cylindrical glass columns (ID = 5.08 cm and L = 30 cm) were used, with open

Table 1
Chemical and physical properties of PAHs and their sediment concentration.

PAH	Chemical structure	S_w[a] (−log M)	D[b] (10^{-6} m^2 s^{-1})	Sediment sample	
				C_{eq}[c] (mg L^{-1})	C_{sed}[d] (mg kg^{-1})
Naphthalene ($C_{10}H_8$)	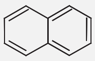	3.06	7.35	9.12	7642
Fluorene ($C_{13}H_{10}$)	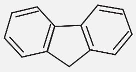	4.08	–	0.226	1411
Phenanthrene ($C_{14}H_{10}$)	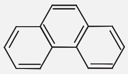	4.46	4.97	1.24	4136
Anthracene ($C_{14}H_{10}$)	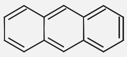	4.48	5.04	0.101	2397
Fluoranthene ($C_{16}H_{10}$)	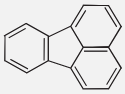	5.08	–	0.04	1326
Pyrene ($C_{16}H_{10}$)	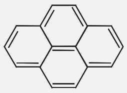	5.35	4.52	0.112	1548

[a] Subcooled liquid solubility (Schwarzenbach et al., 2003).

[b] Diffusivity (Gustafson and Dickhut, 1994).

[c] Equilibrium aqueous concentration.

[d] Concentration extracted from sediment.

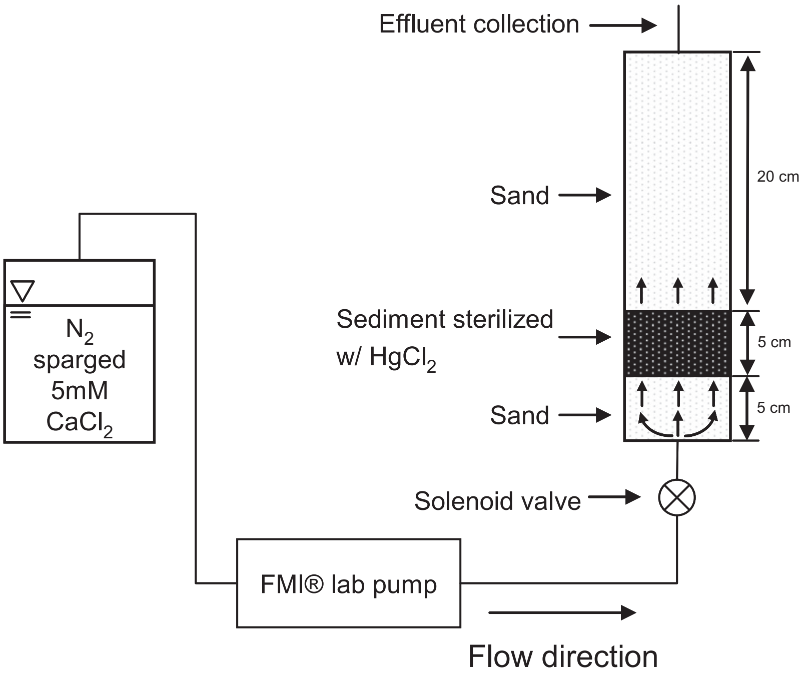

Fig. 1. Skematic of the column experiment apparatus.

beaded columns clamped between aluminum plates, with Teflon seals between the aluminum plates and glass.

The inflow was from the bottom of the column, simulating steady groundwater seepage through the contaminated sediment to the river. Glass frits (5 cm diameter) at the bottom of the column uniformly distributed the upward flow to the sediment layer, reducing the development of preferential flow paths through the sediment. The top aluminum plate was tapped with ¼ – 28 ports to accommodate air tight fittings around 0.16 cm stainless steal tubes. To sample effluent, the other end of the steal tubing pierced the septum of a sealed HPLC sample vial, which was pierced by an additional stainless steel needle to release air pressure from the vial as the aqueous sample accumulated. The influent solution was degassed by N_2 gas purging to reduce oxygen concentration and the column was wrapped with aluminum foil to minimize the effect of oxidative degradation and photodegradation, respectively. Pentafluorobenzoate (PFB^- at 20 mg L^{-1}), was used as an influent tracer and introduced to the bottom of the column emulating groundwater seepage. The pH of the PFB^- and influent solution was adjusted to 7.0 with 0.1 M NaOH.

2.3.1. Column packing

The column was packed with, from bottom to top, 5 cm sand, 5 cm sediment and 20 cm sand (Fig. 1). Prior to packing the sediment layer, non-reactive tracer bromide (Br^-) was spiked into the sediment as potassium bromide crystals at a concentration of 41 mg kg^{-1} and allowed to equilibrate for 7 d for complete dissolution of the KBr into the sediment pore-water. The calculated equilibrium concentration of Br^- in the sediment pore-water was ~60 mg L^{-1}. To operate a column in a sterilized condition, the sediment was also mixed with 4 mmol kg^{-1} $HgCl_2$ (Wolf et al., 1989) prior to packing.

2.3.2. Flow rate settings

A piston pump (Fluid Metering Inc., Syosset, NY) was used to control the flow rate of water into the bottom of the column. The pump and a solenoid valves (Bio-Chem Valve Inc.) were activated with a ChronTrol XT timer (ChronTrol Corporation, San Diego, CA), and a DC power supply provided power to the solenoid valve within an isolated circuit. The piston pump was programmed to operate 1 cycle per 10 or 20 s to supply two different designated volumetric flows of 0.004 or 0.02 mL min^{-1}, respectively. The resulting average Darcy fluxes (q = volumetric flow/cross-sectional area) were 0.284 and 1.42 cm d^{-1}, respectively. The set flow rates were monitored and continued for five or ten pore volumes (PVs) of pumping. The flow rates employed in this experiment approximately encompasses the range of measured flow rate of the site (Hyun et al., 2007). More details about the column and pump settings have been reported elsewhere (Hyun et al., 2006).

2.4. Chemical analysis

For the tracer test, the concentrations of Br^- and PFB^- in the effluent were measured with a Shimadzu HPLC system, equipped with an UV detector set at a monitoring wavelength of 190 nm. A Dionex Ionpac AS14 column (4 mm × 250 mm) and AS4A column (4 mm × 250 mm) were used for Br^- and PFB^- determination, respectively. The PAH concentrations in the sediment extracts (C_{sed}) were determined using a Shimadzu GC–FID system equipped with a DB-5 column. The concentrations of PAH in the effluent solutions (C_{eq} and C^{∞}) were analyzed with an automated Shimadzu HPLC–UV/FL system, equipped with a Supelco PAH column (25 cm × 46 mm, ID, 5 μm particle size). Analytical details for the HPLC–UV/FL and GC–FID conditions have been described elsewhere (Hyun et al., 2006; Jafvert et al., 2006).

3. Results and discussion

3.1. Partitioning of PAHs from sediment to aqueous phase: batch equilibrium experiment

Table 1 shows the concentrations of the six monitored PAHs in the aqueous (C_{eq}) and sediment phase (C_{sed}) measured after batch equilibrium experiments. Assuming that Raoult's law was valid for a given compound (i), the equilibrium aqueous concentration of that compound ($C_{eq,i}$) can be predicted using its subcooled liquid solubility ($S_{w,i}$) and its mole fraction ($x_{o,i}$) in the organic phase (e. g., coal tar):

$$C_{eq,i} = x_{o,i} \times S_{w,i} \tag{1}$$

To apply Eq. (1) to our data, the mole fraction of each compound ($x_{o,i}$) was calculated using three assumptions. First, the total PAH mass extracted by solvents and quantified by GC–FID was assumed to be approximately 60% of the total NAPL mass in the coal tar sediment (Haeseler et al., 1999; Jafvert et al., 2006). Second, the mass-area responses of the many unknown uncalibrated peaks appearing in the GC chromatogram were assumed to be equivalent to the phenanthrene response, whose retention time was located approximately in the middle of the GC chromatogram. Lastly, assuming an average molar mass of all coal tar constituent of 230 g mol^{-1} (Lee et al., 1992), the total number of moles of coal tar was found to be 0.367 mol kg^{-1}, and the mole fractions of naphthalene, fluorene, phenanthrene, anthracene, fluoranthene and pyrene were 0.164, 0.023, 0.064, 0.037, 0.018 and 0.021, respectively.

Inserting the above mole fraction values and solubility data into Eq. (1), the equilibrium aqueous PAH concentrations were calculated and plotted against those actually measured, as shown in Fig. 2. For all six monitored PAH compounds, the actual aqueous concentrations were fairly well predicted, indicating the near ideal solubility behavior of PAHs between the aqueous and coal tar phases in batch mode.

3.2. PAH release from sediment in water seepage system: column experiments

3.2.1. Tracer test

The flow domain of the sediment-sand layer was characterized by analyzing the breakthrough curves (BTCs) of the two non-reactive tracers for two different pore-water velocities. Because the tracer Br$^-$ was spiked into the sediment pore-water while the tracer PFB$^-$ was spiked into the influent solution, different absolute arrival times and response curves were expected. To compare the BTC of each tracer, effluent concentrations were normalized to the initial spiked concentration and potted against the effluent volume expressed in pore volume equivalents.

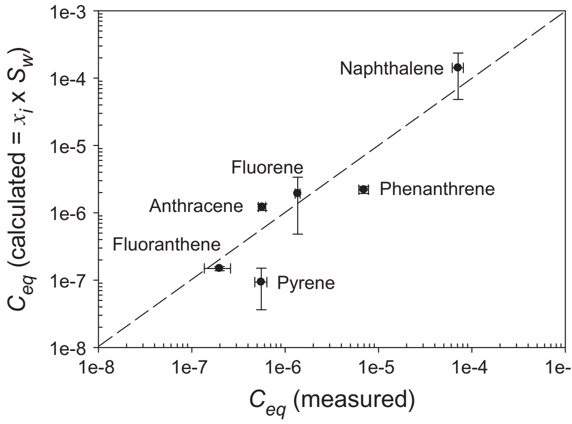

Fig. 2. Measured versus calculated batch equilibrium aqueous concentrations of selected PAHs. Standard deviation of an average value for replicates is shown as an error bar. The dashed line denotes a 1:1 line where ideal dissolution behavior is exhibited.

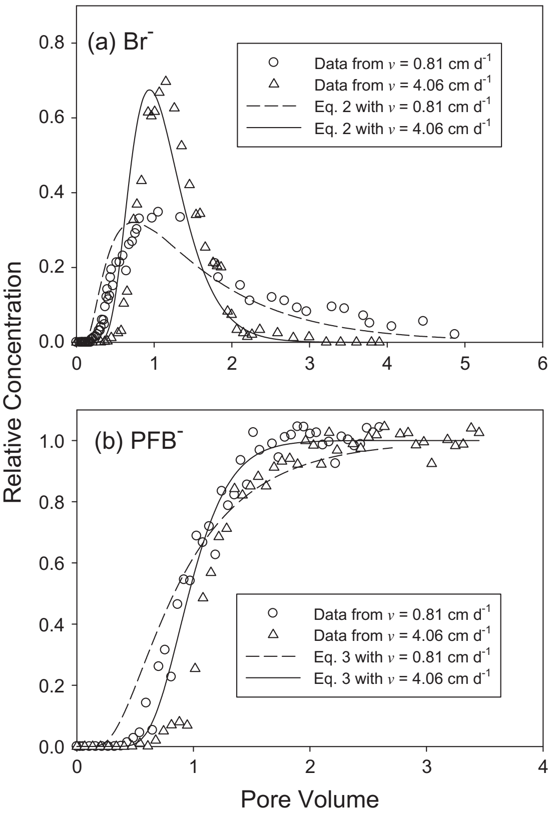

Fig. 3. Relative concentrations of the tracers: (a) bromide, Br$^-$ and (b) pentafluorobenzoate, PFB$^-$ in the column effluent versus effluent volume for two pore-water velocities. Model BTC for Br$^-$ and PFB$^-$ drawn for pore-water velocity of 0.81 and 4.06 cm d^{-1} was shown as dashed and solid lines, respectively.

The BTCs of Br$^-$ measured at two different pore-water velocities are shown in Fig. 3a. In order to find an appropriate solution describing solute transport, it was necessary to specify the initial and the boundary conditions that apply. Given the assumption of an instantaneous injection of a slug of Br$^-$ at the interface of the sediment-sand layer, the BTC curve is predicted, according to Sauty (1980) as:

$$C(x,t) = \frac{M}{\sqrt{4\pi Dt}} \cdot \exp\left[-\frac{(x-vt)^2}{4Dt}\right] \tag{2}$$

where, M = spiked solute mass per cross-sectional area of the sediment-sand layer (mass length^{-2} = 0.00705 kg m^{-2}), D = diffusivity of a solute (length^2 time^{-1} = 6e – 9 m^2 s^{-1}), x = travel distance (length = 0.2 m), v = pore-water velocity (length time^{-1}) and t = time. The solution for slug injection is depicted in Fig. 3a with solid and dashed lines for v = 0.81 and 4.06 cm d^{-1}, respectively.

Even though Br$^-$ was spiked into the sediment pore-water, the theoretical solution for a slug injection at the interface fairly well described the transport pattern of Br$^-$. In addition, the recovery mass estimated by the absolute zeroth spatial momentum (e.g., integration of the area under the measured BTC) accounts for >92% of the initial Br$^-$ addition, indicating that no interaction between the sediment and the Br$^-$ occurred and an evenly distributed upward flow throughout the NAPL-impacted sediment layer. For the BTC obtained under the slow flow regimes, early breakthrough, smaller peak height (i.e., maximum concentration, C_{max}) and greater peak width were observed, likely due to the hydrodynamic dispersion of the tracer within the column. In addition, more spreading of the tracer front at the slow velocity indicates that molecular diffusion must be relatively large compared to mechanical dispersion for the given conditions.

The BTCs of the PFB$^-$ tracer are shown in Fig. 3b. The initial concentration of PFB$^-$ in the column was zero and a constant concentration of PFB$^-$ was added with the influent. The theoretical curve for a continuous solute injection (Eq. (3); Ogata and Banks, 1961) is also shown in Fig. 3b, with solid and dashed lines for slow and fast pore-water velocities, respectively:

$$C(x,t) = \frac{1}{2}C_0 \cdot \left\{ erfc\left[\frac{x - \upsilon t}{\sqrt{4Dt}}\right] + \exp\left(\frac{\upsilon x}{D}\right) \cdot erfc\left(\frac{x + \upsilon t}{\sqrt{4Dt}}\right) \right\} \qquad (3)$$

where C_0 is the tracer concentration being injected and *erfc* is the complementary error function. Similar to the BTCs for Br^-, the early appearance of PFB^- was observed for slower velocity due to the dispersion effect, but the steady-state concentration of PFB^-, equivalent to the input concentration (i.e., $C^* \cong 1$, where C^* is the ratio of effluent concentration to C_0), was achieved after approximately two pore volumes for both pore-water velocities.

The BTCs of the two non-reactive tracers obtained at two different pore-water velocities have implications for the release of PAH from the sediment. (1) Solutes dissolved in the pore-water in the sediment layer are displaced by the influent solution, which can be sufficiently described as a slug injection, (2) the upward groundwater seepage, which is evenly distributed throughout the coal tar-impacted river sediment, can dissolve PAH, and (3) the breakthrough pattern of PAH at the column outlet, which is the result of the combined effects of (1) and (2), will vary with groundwater seepage rates due to the different residence time of seepage water in the sediment layer and the dispersion effect on dissolved PAH.

3.2.2. PAH flux at two different pore-water velocities

3.2.2.1. Slow seepage rate, $v = 0.81$ cm d^{-1}. Under the seepage conditions used in this experiment, no hydraulic mobilization of coal tar (e.g., particle detachment and transport by advective water) from sediment layer was observed. Therefore, the impact of particle-bound PAH or coal tar droplets has not been cited in the interpretation of the experimental data. The BTCs of naphthalene, phenanthrene, anthracene and pyrene in the effluent solutions collected at $v = 0.81$ cm d^{-1} are shown in Fig. 4. During the course of the displacement experiment, the total mass of all four PAHs depleted from the NAPL-impacted sediment was found to be negligible based on the mass balance calculation, due to the extremely high PAH concentrations initially present in the sediment (Table 1) and the relatively low volume of influent pumped (e.g., 0.7–1.9 L). For example, only 0.21% of the naphthalene initially present in the sediment layer was released. Mass depletions of all other PAHs were less than 0.009%. Hence, a relatively constant source, in terms of NAPL composition (e.g., PAH concentration) in the sediment, can be assumed to have been retained during these experiments.

Similar to the results of the PFB^- tracer tests, the first notable trend in the slow flow rate data was that steady-state conditions were achieved after approximately 2–3 pore volumes of flow, after which, near constant release of each of the four PAHs was observed. The average retention time of seepage water within the 5 cm sediment layer was approximately 17 d under the given flow conditions. A second observation was the wide variation in the observed steady-state concentrations among the compounds. Theoretically, the steady-state concentration (C^∞) in the column effluent should be equal to C_{eq} of the batch experiment if the seepage water sufficiently reacts with the coal tar phase to reach dissolution equilibrium. The monitored steady-state PAH concentration, as shown in Fig. 4, was a result of a 'pseudo-steady-state' between the flowing water and the coal tar phase; henceforth, called the pseudo-steady-state concentration. The pseudo-steady-state concentrations (C^∞) were approximately: 7.0 mg L^{-1} naphthalene, 5.0×10^{-1} mg L^{-1} phenanthrene, 2.7×10^{-2} mg L^{-1} anthracene and 1.0×10^{-2} mg L^{-1} pyrene, which are approximately equivalent to 75%, 43%, 26% and 9% of the respective C_{eq} measured in batch experiments (C_{eq}, Table 1). The ratio of C^∞ to C_{eq} for all PAHs was found to decrease in the order of decreasing subcoolded liquid solubility. The lower steady-state concentration of each PAH in the effluent solution compared their batch equilibrium concentration, as well as the relationship with its solubility, indicates that dissolution equilibrium between the influent and sediment phase was not attained within the contact time provided by the pore-water velocity of 0.81 cm d^{-1}.

Dissolution may be both thermodynamically and kinetically limited. The dissolution kinetics of a multi-component NAPL mixture will be influenced by several factors including the rate-limited

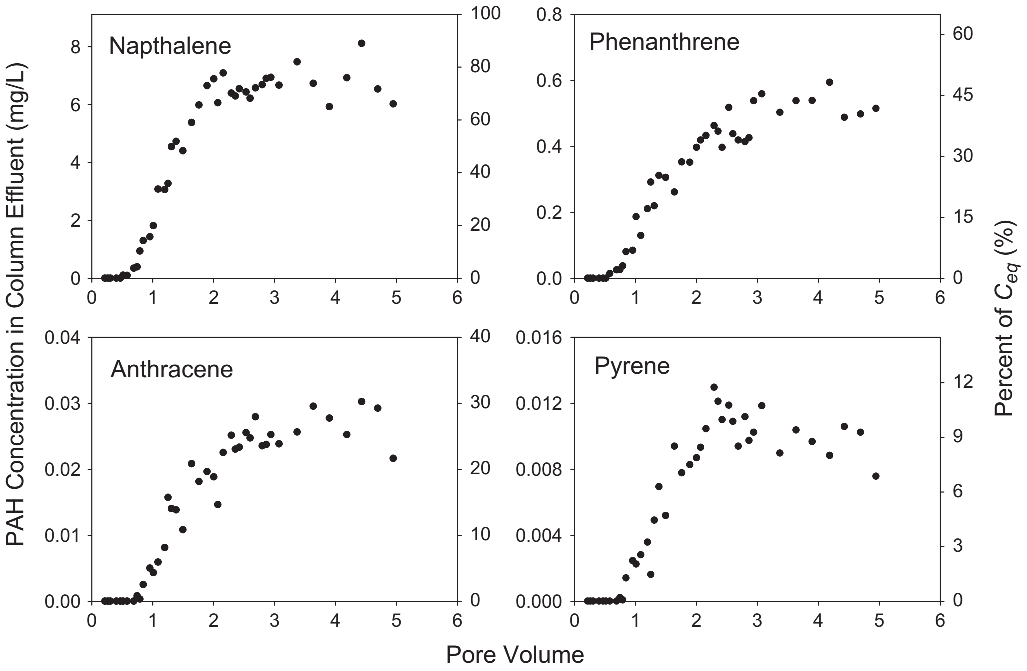

Fig. 4. The PAH concentrations (left y-axis) in the effluent collected at a pore-water velocity of 0.81 cm d^{-1}. The right y-axis denotes the percentage of the PAH concentration in the effluent relative to the batch equilibrium concentration (C_{eq}).

process at the NAPL–water interface (Powers et al., 1991; Borden and Kao, 1992), inhibition of intra-NAPL diffusion (Brahma and Harmon, 2003) and the composition of the NAPL mixture (Lee et al., 1992). A greater tendency toward nonequilibrium mass transfer would be expected for a certain NAPL conditions such as a larger NAPL size (i.e., small NAPL–water interface), higher pore-water velocity (Heyse et al., 1997) and lower NAPL saturation, all of which may cause dissolution to be kinetically limited. In this displacement experiment with coal tar-contaminated sediment, the dissolution of PAH is likely to have been limited by both the small sediment–water interface and the contact time between the coal tar and pore-water.

3.2.2.2. Fast seepage rate, $v = 4.06\ \mathrm{cm\ d^{-1}}$. Under the condition of rate-limited nonequilibrium dissolution an increase in the flow rate (i.e., reduced contact time) should induce a reduction in the steady-state effluent concentrations of solute. To investigate this effect, a displacement experiment with a newly packed sediment column was conducted at the elevated pore-water velocity of 4.06 cm $\mathrm{d^{-1}}$ (retention time = approximately 3.5 d). The concentration profiles of the four PAHs in the column effluents plotted as a function of the pore volume displaced are shown in Fig. 5.

There were two notable differences from the result with the slower seepage rate. First, reduced pseudo-steady-state concentrations (C^{∞}) of PAH were observed; 2.5 mg $\mathrm{L^{-1}}$ naphthalene, 0.2 mg $\mathrm{L^{-1}}$ phenanthrene, 6.1×10^{-3} mg $\mathrm{L^{-1}}$ anthracene and 3.4×10^{-3} mg $\mathrm{L^{-1}}$ pyrene. These were about 20–30% of the C^{∞} values measured under the lower pore-water velocity conditions, which can be attributed to the shorter reaction time due to the faster pore-water velocity. Furthermore, larger pore volumes (e. g., 7–8 PVs) were required to reach pseudo-steady-state conditions. The observation is consistent with the result from our previous work (Hyun et al., 2006), where effect of pore-water velocity on effluent PAH concentration displacing from coal tar-contaminated sediment was investigated. Upon increasing pore-water velocity was increased from 2.04 cm $\mathrm{d^{-1}}$ to 10.2 cm $\mathrm{d^{-1}}$ during a portion of displacement experiment, time required to reach new steady-state concentration was extended (e.g., $\geqslant$6 PVs) and steady-state concentration of PAH was dropped in one-half. Those are all evidence of the kinetically limited dissolution of PAHs from the sediment phase. Secondly, an initial high concentration (so-called, first flush export) was observed between 2 and 5 PVs, but this decreased after a few more pore volumes. Before starting upward flow, the PAH concentration in the sediment pore-water should be near that of the batch equilibrium concentration (C_{eq}), assuming a local dissolution equilibrium (e.g., $\cong x_{i,o} \times S_{w,L}$). At the onset of upward flow, PAH-free influent will displace the pore-water containing PAHs. A new nonequilibrium, steady-state condition, which is rate-dependent, will be established between the advancing PAH-free solution and the sediment phase.

Conceptual model of PAH flux from the sediment can be proposed by the initial high export (i.e., first flush) and the constant export of PAH, which is determined by a new nonequilibrium. The general PAH breakthrough pattern from coal tar-impacted sediment shown in Fig. 5 was described by superimposing these two analytical solutions using two parameters for each PAH, M in Eq. (2) and C_0 in Eq. (3), which are the solute mass dissolved in sediment pore-water and the pseudo-steady-state concentration (C^{∞}), respectively. As noted earlier, the peak height of a slug injection (C_{max} from Eq. (2)) is proportional to the pore-water velocity, while the steady-state concentration of nonequilibrium dissolution (C^{∞} in Eq. (3)) is inversely proportional to the pore-water velocity. Therefore, the appearance of an initial bulge at the faster pore-water velocity (Fig. 6a) is due to the superimposition of two curves, one exhibiting a high C_{max} and the other, a small C^{∞}. In contrast, no initial bulge was observed under the slower pore-water velocity (Fig. 6b) due to the smaller contrast between C^{∞} and C_{max}.

3.2.2.3. PAH mass flux under different seepage rate. Chemical mass flux carried by the flowing water can be estimated by the water flux and the concentration of solutes dissolved in flowing water. Therefore, the total PAH mass flux (J_T, mass · $\mathrm{area^{-1}\ time^{-1}}$) advectively transported from sediment can be determined by multiplying the rate of groundwater seepage (q_w) through the sediment layer and the sum of the PAH steady-state concentrations (ΣC^{∞}); $J_T = q_w \times \Sigma C^{\infty}$, and q_w and ΣC^{∞} are inversely proportional each

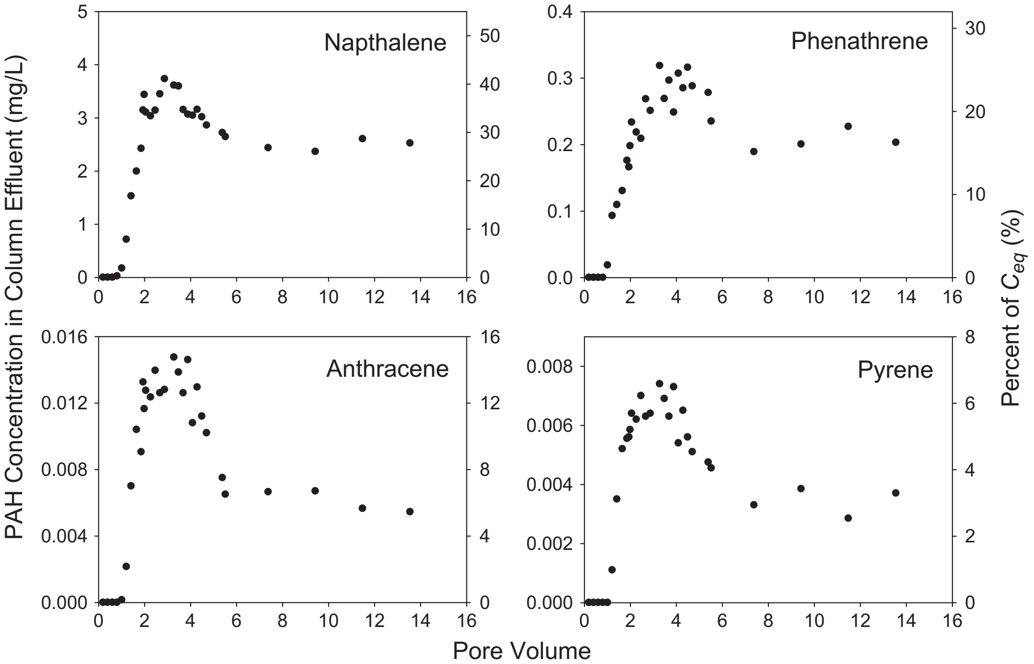

Fig. 5. The PAH concentrations (left y-axis) in the effluent collected at a pore-water velocity of 4.06 cm $\mathrm{d^{-1}}$. The right y-axis denotes the percentage of the PAH concentration in the effluent relative to the batch equilibrium concentration (C_{eq}).

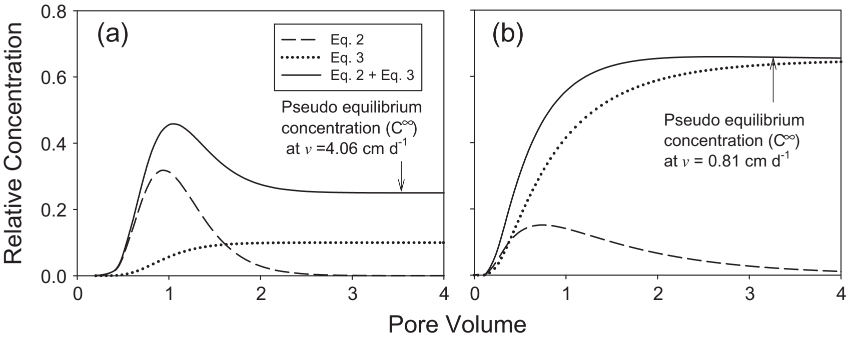

Fig. 6. Naphthalene concentration in the effluent collected at a pore-water velocity of 4.06 cm d^{-1} (closed circles) and the theoretical model breakthrough curve (solid line) derived as the addition of a slug injection curve (Eq. (2), dotted line) and a continuous input curve (Eq. (3), dashed line).

other. The seepage water flux (q_w) is driven by the vertical hydraulic head gradient through sediment layer (e.g., higher hydraulic water head at the bottom of the sediment layer than at sediment–water interface). At the slow seepage rate of 0.81 cm d^{-1}, chemical flux of each PAH (J) through the sediment layer was determined as 49.7, 3.55, 0.192, and 0.007 mg m^{-2} d^{-1} for naphthalene, phenanthrene, anthracene, and pyrene, respectively. At the fast seepage rate of 4.06 cm d^{-1}, the determined chemical flux for naphthalene, phenanthrene, anthracene, and pyrene was 71.0, 5.68, 0.173, and 0.097 mg m^{-2} d^{-1}. Total flux (J_T) of measured PAHs was 53.5 and 77 mg m^{-2} d^{-1} for slow and fast seepage rate, respectively. Note that the flux change of each PAH was not identical to the change of effluent concentrations due to the concurrent consideration of the change of seepage rates. That is, slow seepage water may carry greater amount of dissolved PAH but export lower amount of PAH because of smaller volume of discharge. Total PAH mass flux through coal tar-impacted river sediment highly depends on time-dependent reaction between seepage water and sediment which will be essentially controlled by hydraulic head gradient through sediment layer.

3.3. Summary

Equilibrium partitioning and the fluxes of several PAHs from coal tar-impacted sediment toward river water were measured on a laboratory scale. The equilibrium partitioning (C_{eq}) of six PAHs (naphthalene, fluorene, phenanthrene, anthracene, fluoranthene and pyrene) between coal tar-impacted sediment and water can be estimated using a Raoult's law approach. In a 1-D seepage experiment, the flux of selected PAHs at the sediment interface was interpreted by the first flush, followed by the rate-limited release. All six PAHs displayed evidence of nonequilibrium dissolution from the coal tar-impacted sediment which was most out of equilibrium at higher seepage flow rates. The PAH mass flux from coal tar-impacted sediment toward overlaying water body was found seepage rate-dependent (i.e., time). Therefore, the results obtained in this study suggest that, to assess the environmental risk posed by coal tar-impacted river sediment, and to deploy appropriate remediation strategies for the contaminated sites, it is important to understand both thermodynamic (equilibrium) and kinetic (nonequilibrium) controls on PAH dissolution and release from the sediment.

References

Borden, R.C., Kao, C.-M., 1992. Evaluation of groundwater extraction for remediation of petroleum-contaminated aquifers. Water Environ. Res. 64, 28–36.

Brahma, P.P., Harmon, T.C., 2003. The effect of multi component diffusion on NAPL dissolution from spherical ternary mixtures. J. Contam. Hydrol. 67, 43–60.

Gustafson, K.E., Dickhut, R.M., 1994. Molecular diffusivity of polycyclic aromatic hydrocarbons in aqueous solution. J. Chem. Eng. Data 39, 281–285.

Haeseler, F., Blanchet, D., Druelle, V., Werner, P., Vandecasteele, J.-P., 1999. Analytical characterization of contaminated soils from former manufactured gas plant. Environ. Sci. Technol. 33, 825–830.

Haritash, A.K., Kaushik, C.P., 2009. Biodegradation aspects of polycyclic aromatic hydrocarbons (PAHs): a review. J. Hazard. Mater. 169, 1–15.

Heyse, E., Dai, D., Rao, P.S.C., Delfino, J.J., 1997. Development of a continuously stirred flow cell for investigation sorption mass transfer. J. Contam. Hydrol. 25, 337–355.

Heyse, E., Augustijn, D., Rao, P.S.C., Delfino, J.J., 2002. Nonaqueous phase liquid dissolution and organic matter sorption in porous media: review of system similarities. CRC Crit. Rev. Environ. Sci. Technol. 32, 337–397.

Hunt, J.R., Sitar, N., Udell, K.S., 1988a. Nonaqueous phase liquid transport and cleanup: 1. Analysis of mechanisms. Water Resour. Res. 25, 1247–1258.

Hunt, J.R., Sitar, N., Udell, K.S., 1988b. Nonaqueous phase liquid transport and cleanup, 2. Experimental studies. Water Resour. Res. 24, 1259–1269.

Hyun, S., Jafvert, C.T., Lee, L.S., Rao, P.S.C., 2006. Laboratory studies to characterize the efficacy of a sand capping a tar-contaminated sediment. Chemosphere 63, 1879–1893.

Hyun, S., Jafvert, C.T., Jenkinson, B., Enfield, C., Johnson, B., 2007. Measuring the flux at the interface of coal-tar impacted sediment and river water near a former MGP site. Chemosphere 68, 1020–1029.

Jafvert, C.T., Lane, D., Lee, L.S., Rao, P.S.C., 2006. Partitioning of mono- and polycyclic hydrocarbons in a river sediment adjacent to a former manufactured gas plant site. Chemosphere 62, 315–321.

Lee, K.Y., Chrysikopoulos, C.V., 2006. Dissolution of a multicomponent DNAPL pool in an experimental aquifer. J. Hazard. Mater. 128, 218–226.

Lee, L.S., Rao, P.S.C., Okuda, I., 1992. Equilibrium partitioning of polycyclic aromatic hydrocarbons from coal tar into water. Environ. Sci. Technol. 26, 2110–2115.

Luthy, R.G., Ramaswami, A., Ghoshal, S., Merkel, W., 1993. Interfacial films in coal-tar nonaqueous-phase liquid water-system. Environ. Sci. Technol. 27, 2914–2918.

Luthy, R.G., Dzombak, D.A., Peters, C.A., Roy, S.B., Ramaswami, A., Nakeles, D.V., Nott, B.R., 1994. Remediating tar-contaminated soils at manufactured gas plant sites. Environ. Sci. Technol. 28, 266A–276A.

Mahjoub, B., Jayr, E., Bayard, R., Gourdon, R., 2000. Phase partition of organic pollutants between coal tar and water under variable experimental conditions. Water Res. 34, 3551–3560.

Nambi, I.M., and Powers, S.E., 2003. Mass transfer correlations for nonaqueous phase liquid dissolution from regions with high initial saturations. Water Resour. Res. doi:10.1029/20021WR000667.

Ogata, A., Banks, R.B., 1961. A Solution of the Differential Equation of Longitudinal Dispersion in Porous Media. US Geological Survey, Professional Paper 411-A.

Powers, S.E., Loureiro, C.O., Abriola, L.M., Weber, W.J., 1991. Theoretical-study of the significance of nonequilibrium dissolution of nonaqueous phase liquid in subsurface systems. Water Resour. Res. 27, 463–477.

Sauty, J.-P., 1980. An analysis of hydrodispersive transfer in aquifers. Water Resour. Res. 16, 145–158.

Schwarzenbach, R.P., Gschwend, P.M., Imboden, D.M., 2003. Environmental Organic Chemistry. John Wiley, New York.

Seagren, E.A., Moore, T.O., 2003. Nonaqueous phase liquid pool dissolution as a function of average pore water velocity. J. Environ. Eng. ASCE 129, 786–799.

Totsche, K.U., Jann, S., Kögel-Knabner, I., 2006. Release of polycyclic aromatic hydrocarbons, dissolved organic carbon, and suspended matter from disturbed NAPL-contaminated gravelly soil material. Vadose Zone J. 5, 469–479.

Wolf, D.C., Dao, T.H., Scott, H.D., Lavy, T.L., 1989. Influence of sterilization methods on selected microbiological, physical, and chemical soil properties. J. Environ. Qual. 18, 39–44.